Electronic Supplementary Material (ESI) for Journal of Materials Chemistry A.

Tetragonal-Structured Anisotropic 2D Metal Nitride Monolayers and Their Halides with Versatile Promises in Energy Storage and Conversion

Xu Zhang, Zihe Zhang, Xudong Zhao, Dihua Wu, Xin Zhang, Zhen Zhou*

Tianjin Key Laboratory of Metal and Molecule Based Material Chemistry, Computational Centre for Molecular Science, Institute of New Energy Material Chemistry, Collaborative Innovation Center of Chemical Science and Engineering (Tianjin), School of Materials Science and Engineering, National Institute for Advanced Materials, Nankai University, Tianjin 300350, P. R. China. *E-mail: zhouzhen@nankai.edu.cn

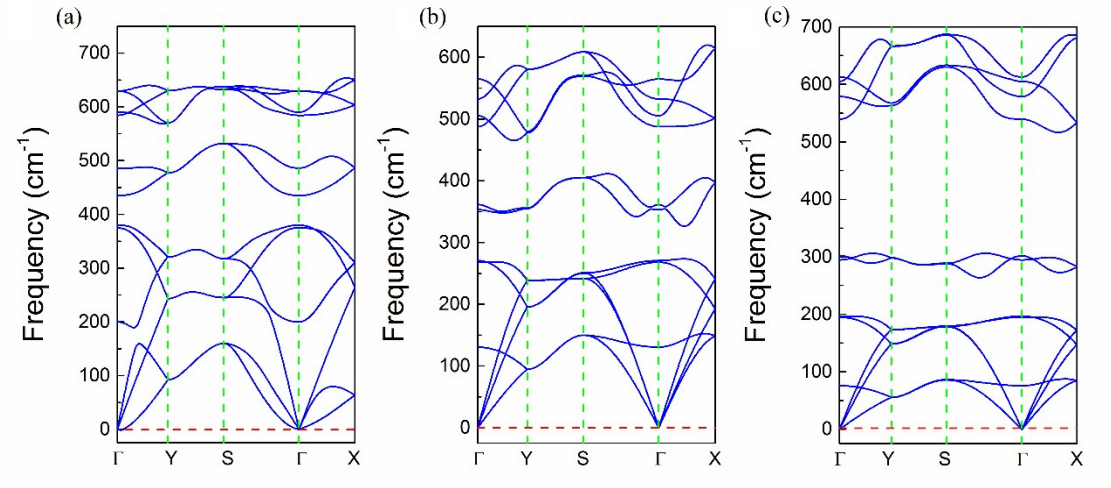

Fig. S1 Phonon band dispersion of (a) t-TiN; (b) t-ZrN and (c) t-HfN monolayer calculated through DFPT as implemented in PHONOPY code.

Table S1. The bond length (Å) of Ti-N, Zr-N and Hf-N along the x and y direction, respectively.

	Ti-N	Zr-N	Hf-N
x	2.00	2.15	2.12
y	2.04	2.22	2.16

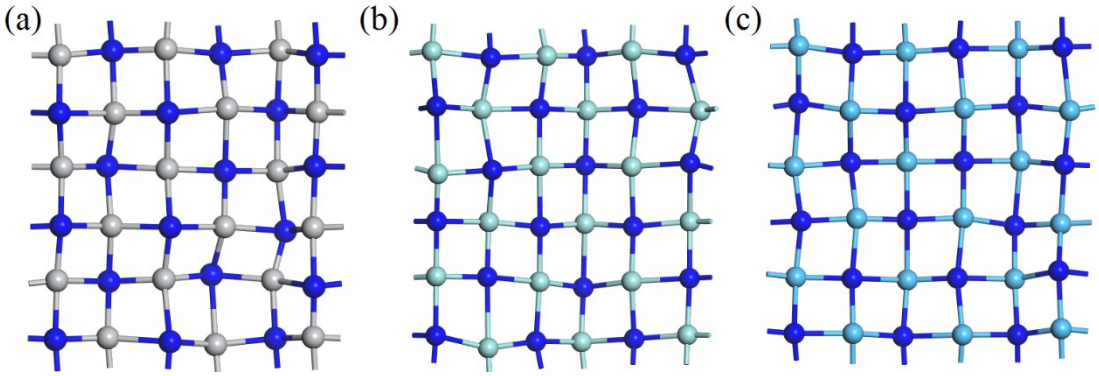

Fig. S2 The snapshot of the equilibrium structure of (a) t-TiN; (b) t-ZrN and (c) t-HfN at 1500 K at the end of 5 ps first-principles molecular dynamic (MD) simulation. A 3×3 supercell was adopted to approximate the realistic stability.

The in-plane stiffness was calculated by $C_{2D} = (\partial^2 E_{total}/\partial \varepsilon^2)/S_0$, where E_{total}, ε and S_0 represent the total energy per unit cell, uniaxial strain and the area of the optimized unit cell, respectively, and the results are summarized in Table S2. The gravity induced out of plane deformation h can be calculated by $h/l \approx (\rho g l/C_{2D})^{1/3}$ [1], where l is the length of the monolayer, ρ is the density (Table S2) and g is the gravitational acceleration.

Through the elasticity theory, the gravity induced out of plane deformation h can be estimated. Assuming the length of the monolayer to be 100 μm, the order of magnitude of h/l is ~10^{-4}, which indicates that the t-MN monolayers behave sufficient rigidity to form freestanding 2D monolayers without substrates.

Table S2. The in-plane stiffness C_{2D} (N/m) and density ρ (10^{-6} kg/m^2) of MN (M = Ti, Zr, Hf).

	TiN	ZrN	HfN
$C_{2D}(x)$	46.4	30.5	44.2
$C_{2D}(y)$	163.6	210.3	194.1
ρ	1.43	2.05	3.64

Table S3. The charge transfer c.t. (|e|) of t-MN (M = Ti, Zr, Hf).

	TiN	ZrN	HfN
c.t. (M)	–1.48	–1.61	–1.67
c.t. (N)	1.48	1.61	1.67

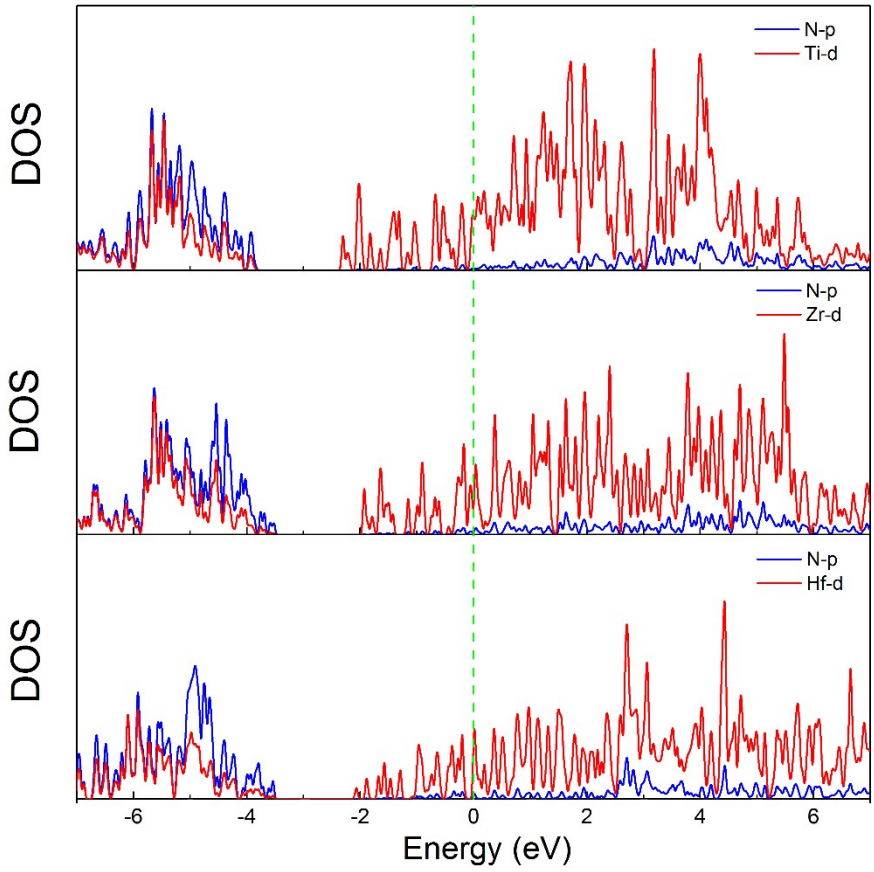

Fig. S3 The partial density of states (PDOS) of (a) t-TiN, (b) t-ZrN, and (c) t-HfN.

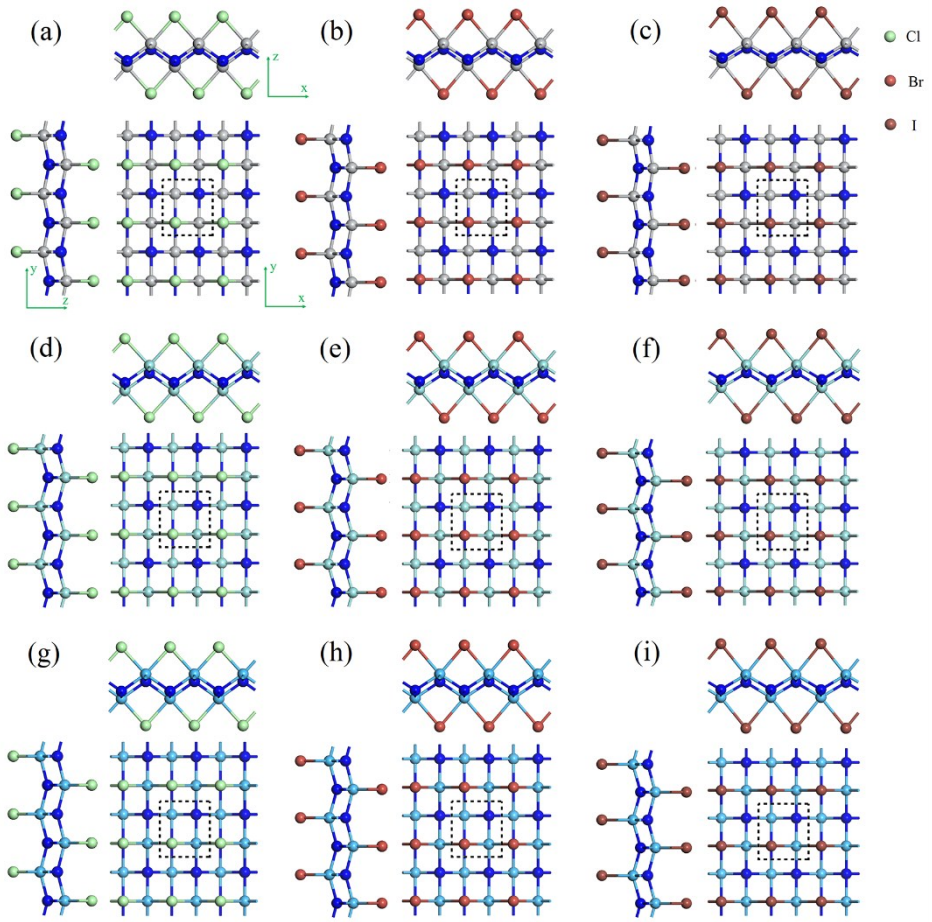

Fig. S4 Structure schematics of (a) t-TiNCl, (b) t-TiNBr, (c) t-TiNI, (d) t-ZrNCl, (e) t-ZrNBr, (f) t-ZrNI, (g) t-HfNCl, (h) t-HfNBr, and (i) t-HfNI. Dashed rectangles represent the unit cell.

Table S4. The bond length (Å) of t-MNX (M = Ti, Zr, Hf, X = Cl, Br, I) monolayers.

	TiNCl	TiNBr	TiNI	ZrNCl	ZrNBr	ZrNI	HfNCl	HfNBr	HfNI
M-N (x)	2.00	2.02	2.04	2.16	2.16	2.18	2.12	2.13	2.14
M-N (y)	2.01	2.01	2.01	2.16	2.16	2.16	2.13	2.13	2.13
M-X	2.45	2.60	2.80	2.62	2.76	2.96	2.59	2.74	2.94

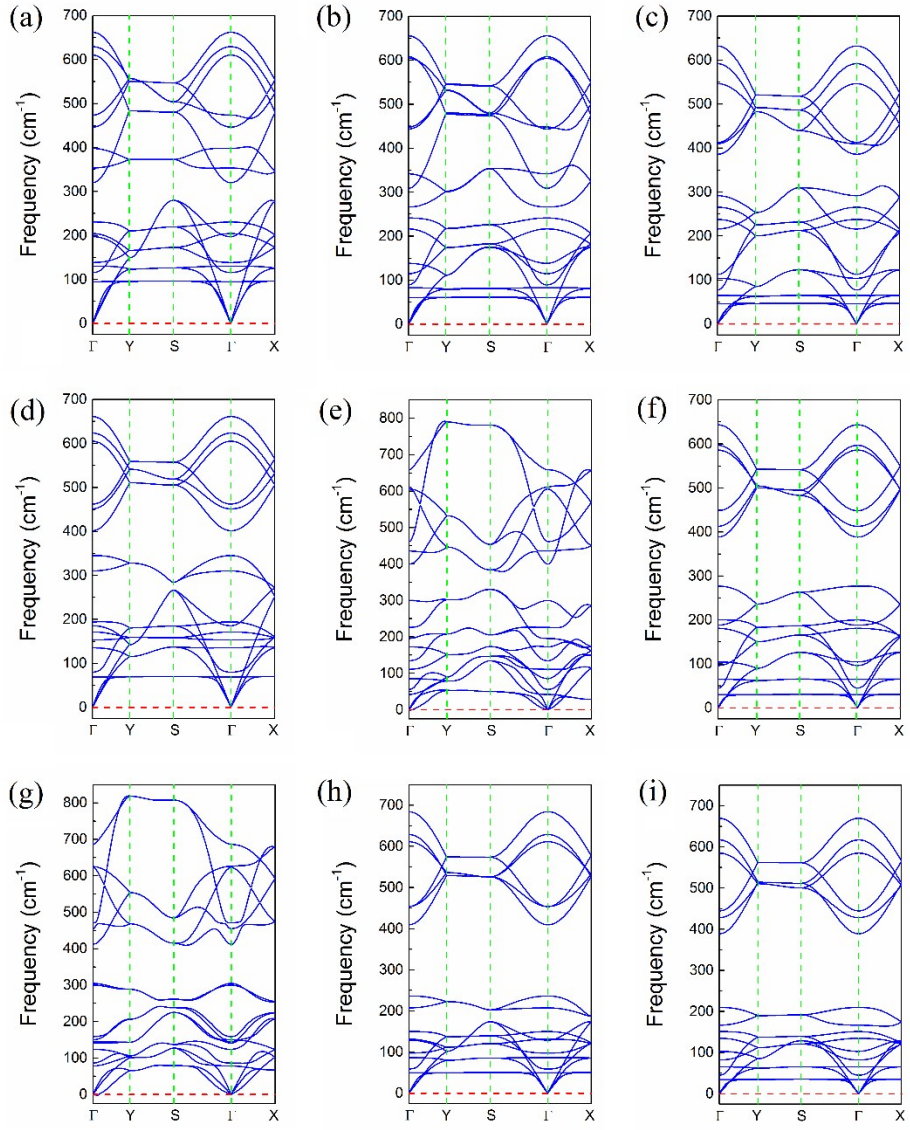

Fig. S5 Phonon band dispersion of (a) t-TiNCl, (b) t-TiNBr, (c) t-TiNI, (d) t-ZrNCl, (e) t-ZrNBr, (f) t-ZrNI, (g) t-HfNCl, (h) t-HfNBr, and (i) t-HfNI.

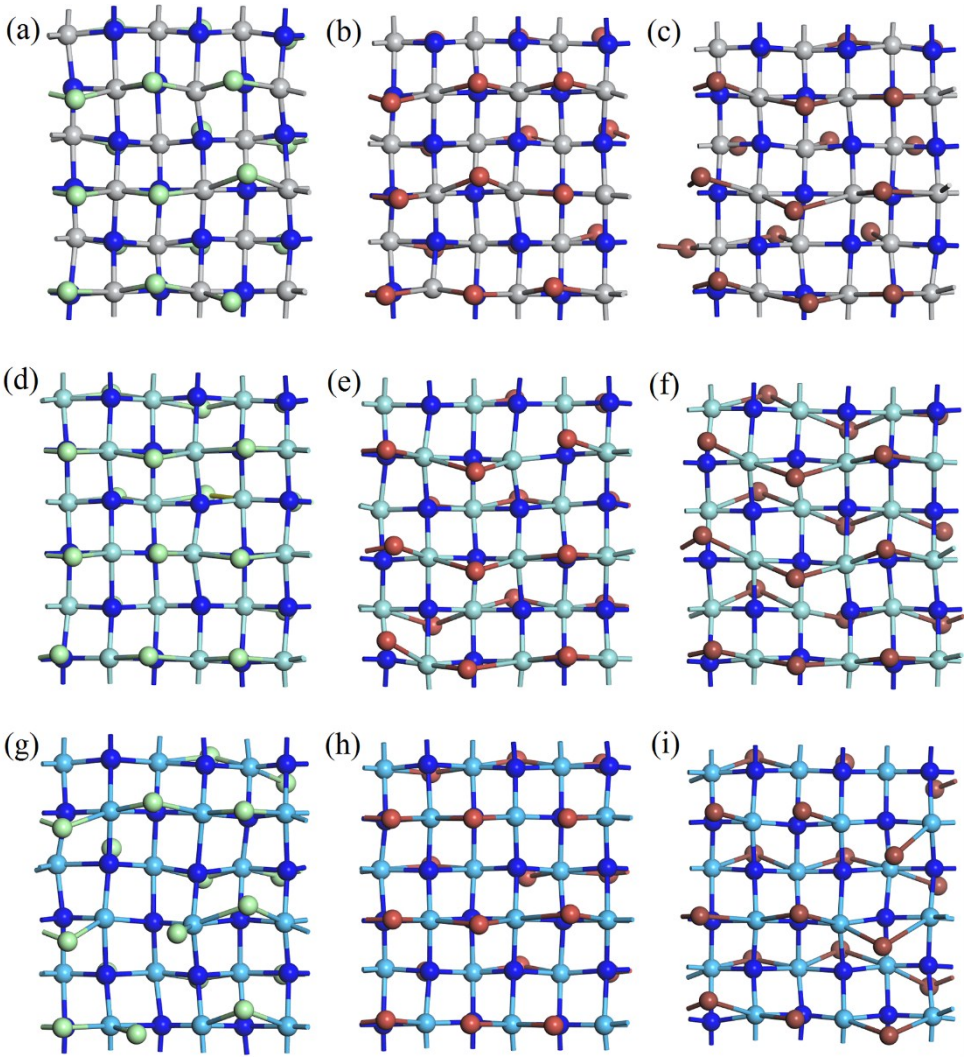

Fig. S6 The snapshot of the equilibrium structure of (a) t-TiNCl, (b) t-TiNBr, (c) t-TiNI, (d) t-ZrNCl, (e) t-ZrNBr, (f) t-ZrNI, (g) t-HfNCl, (h) t-HfNBr, and (i) t-HfNI at the end of 5 ps first-principles molecular dynamic (MD) simulation at 800 K.

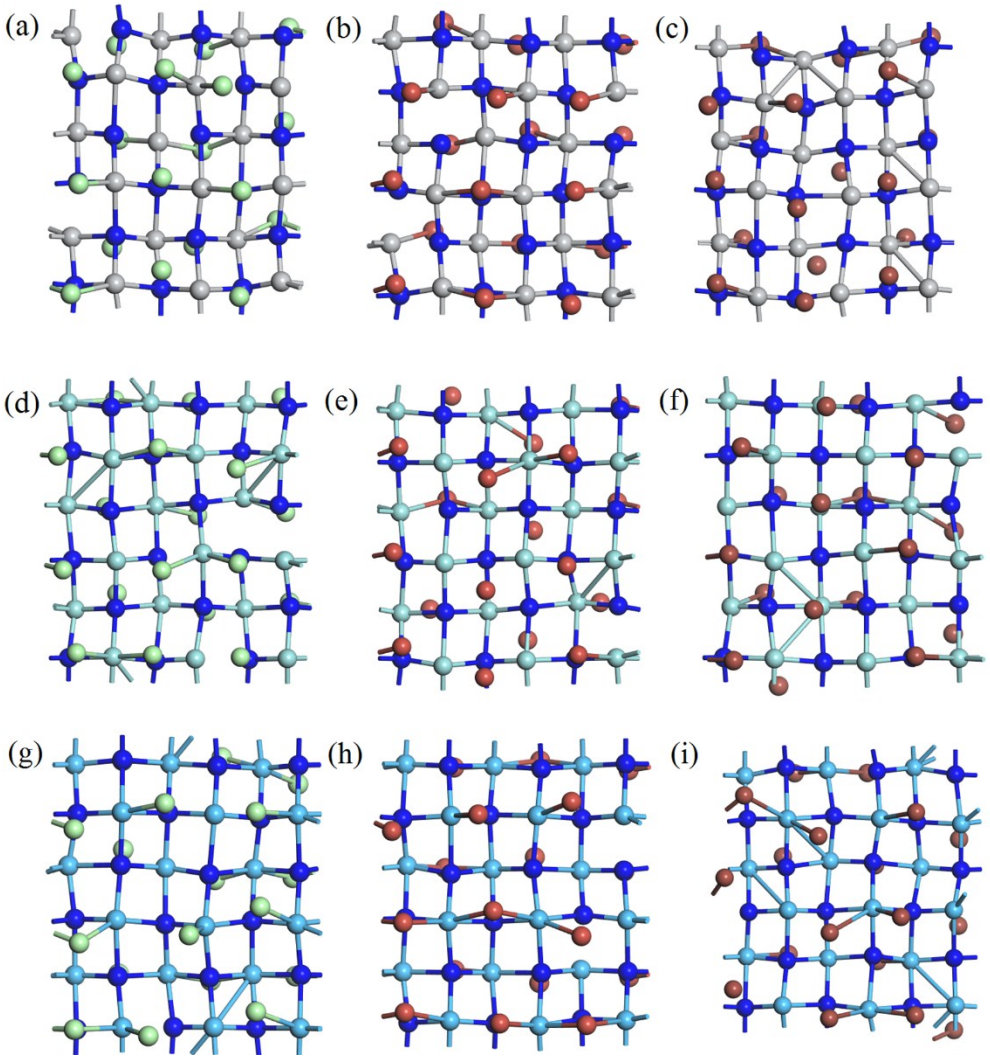

Fig. S7 The snapshot of the equilibrium structure of (a) t-TiNCl, (b) t-TiNBr, (c) t-TiNI, (d) t-ZrNCl, (e) t-ZrNBr, (f) t-ZrNI, (g) t-HfNCl, (h) t-HfNBr, and (i) t-HfNI at the end of 5 ps first-principles molecular dynamic (MD) simulation at 1500 K.

Table S5. The band gaps G (eV) with and without SOC, position of VBM and CBM for t-MNX (M = Ti, Zr, Hf, X = Cl, Br, I) monolayers.

	TiNCl	TiNBr	TiNI	ZrNCl	ZrNBr	ZrNI	HfNCl	HfNBr	HfNI
G	1.42	1.40	0.41	2.80	2.77	2.25	3.26	3.22	2.68
G (SOC)	1.41	1.40	0.35	2.81	2.79	2.12	3.26	3.22	2.62
VBM	Γ	Γ	Γ	Γ	Γ	Γ	Γ	Γ	Γ
CBM	Γ	Γ	Γ	Γ	Γ	Γ	Γ	Γ	Γ
	direct	direct	direct	direct	direct	direct	direct	direct	direct

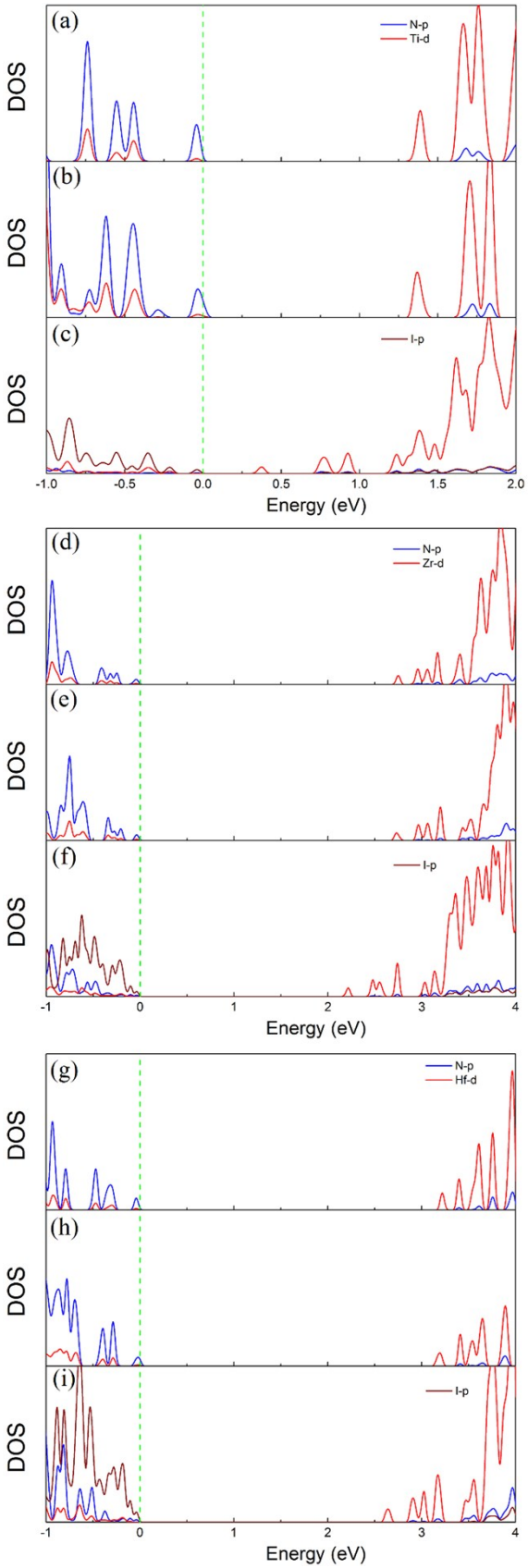

Fig. S8 PDOS of (a) t-TiNCl, (b) t-TiNBr, (c) t-TiNI, (d) t-ZrNCl, (e) t-ZrNBr, (f) t-ZrNI, (g) t-HfNCl, (h) t-HfNBr, and (i) t-HfNI.

For t-MNCl and t-MNBr monolayers, the hybridization of N-*p* and M-*d* orbitals dominantly contributes to the states near Fermi level which reveals that their bonding states are mainly contributed by the hybridization of N-*p* and M-*d*. However, for t-MNI, the states near VBM are dominantly contributed by I-*p* and N-*p* while the states near CBM are mainly contributed by the hybridization of N-*p* and M-*d*.

Table S6. The absolute value of effective mass |m*| (m_0, the mass of free electrons). The subscript e, h, x and y represent electron, hole, x and y directions, respectively.

	TiNCl	TiNBr	TiNI	ZrNCl	ZrNBr	ZrNI	HfNCl	HfNBr	HfNI
$\|m_e^*\|_x$	0.52	0.44	0.36	0.56	0.47	0.38	0.67	0.50	0.38
$\|m_h^*\|_x$	0.38	0.36	0.20	0.42	0.44	0.22	0.42	0.42	0.28
$\|m_e^*\|_y$	0.46	0.42	0.36	0.36	0.35	0.32	0.33	0.32	0.30
$\|m_h^*\|_y$	0.24	0.28	1.33	0.51	0.62	1.89	0.35	0.43	2.12

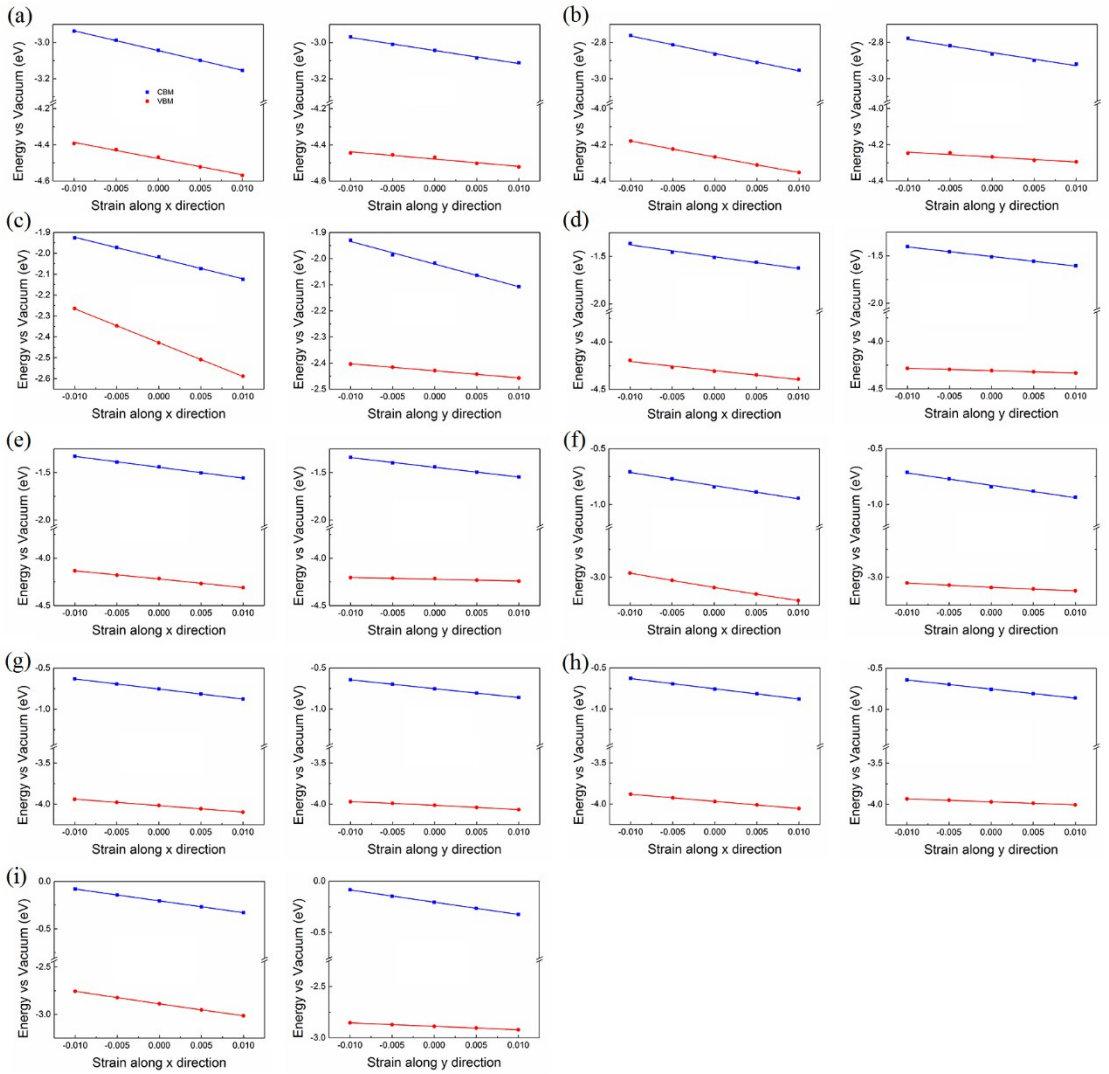

Fig. S9 The CBM and VBM position of (a) t-TiNCl, (b) t-TiNBr, (c) t-TiNI, (d) t-ZrNCl, (e) t-ZrNBr, (f) t-ZrNI, (g) t-HfNCl, (h) t-HfNBr, and (i) t-HfNI with respect to the vacuum level as a function of the uniaxial strain ε along the x and y direction. The solid lines are the linear fitting to the data.

Table S7. The absolute value of DP constant E_1 (eV) of t-MNX.

	TiNCl	TiNBr	TiNI	ZrNCl	ZrNBr	ZrNI	HfNCl	HfNBr	HfNI
$\|E_{1e}\|_x$	10.9	9.6	9.9	11.0	11.5	11.8	12.3	12.5	12.4
$\|E_{1h}\|_x$	8.9	8.7	16.2	8.3	8.8	12.3	7.9	8.7	12.9
$\|E_{1e}\|_y$	7.2	8.1	8.7	10.1	10.2	11.1	10.8	11.0	11.9
$\|E_{1h}\|_y$	4.0	4.1	2.7	2.5	1.8	3.4	4.9	3.6	3.4

Table S8. The in-plane stiffness C_{2D} (N/m) of t-MNX along the x and y direction.

	TiNCl	TiNBr	TiNI	ZrNCl	ZrNBr	ZrNI	HfNCl	HfNBr	HfNI
C_{2Dx}	150.3	147.5	143.0	140.7	135.7	136.3	153.9	148.5	148.7
C_{2Dy}	167.7	168.8	179.2	132.0	126.0	122.9	153.4	146.1	141.8

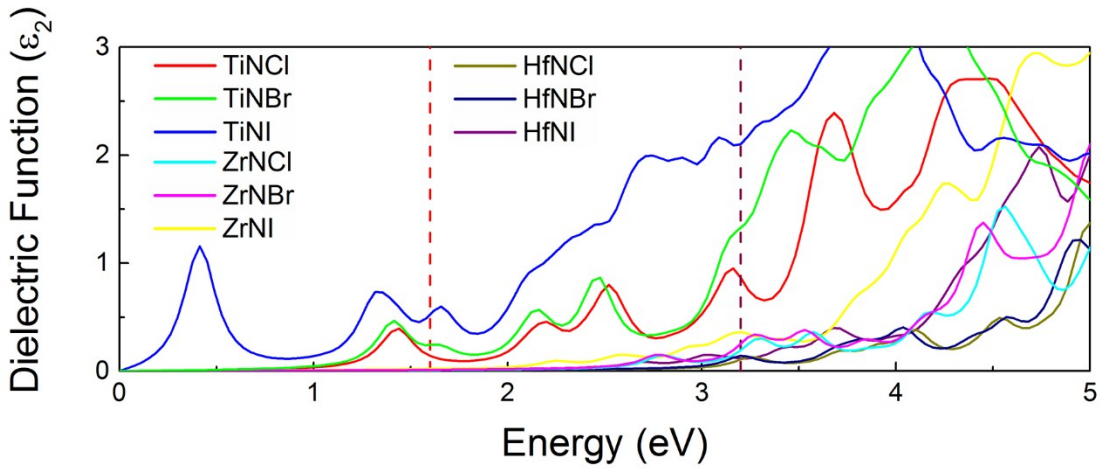

Fig. S10 Computed imaginary dielectric functions versus energy for t-MNX monolayers. The $\varepsilon_2(\omega)$ terms are the average of x, y and z directions, that is to say, $\varepsilon_2(\omega) = 1/3(\varepsilon_{xx}(\omega)+ \varepsilon_{yy}(\omega)+\varepsilon_{zz}(\omega))$. The area between the red and purple lines represents the visible range.

Table S9. Calculated carrier mobility μ (cm^2 V^{-1} S^{-1}) of t-MNX along the x and y directions.

	TiNCl	TiNBr	TiNI	ZrNCl	ZrNBr	ZrNI	HfNCl	HfNBr	HfNI
μ_e (x)	65.3	118.6	158.6	52.9	66.4	96.4	31.9	54.4	93.3
μ_h (x)	186.3	211.8	200.2	163.8	126.6	272.0	197.1	156.4	162.5
μ_e (y)	218.1	210.7	261.6	139.4	138.6	135.1	167.1	161.1	153.2
μ_h (y)	2450.1	1759.8	197.8	1149.3	1326.7	40.8	739.7	851.4	38.8

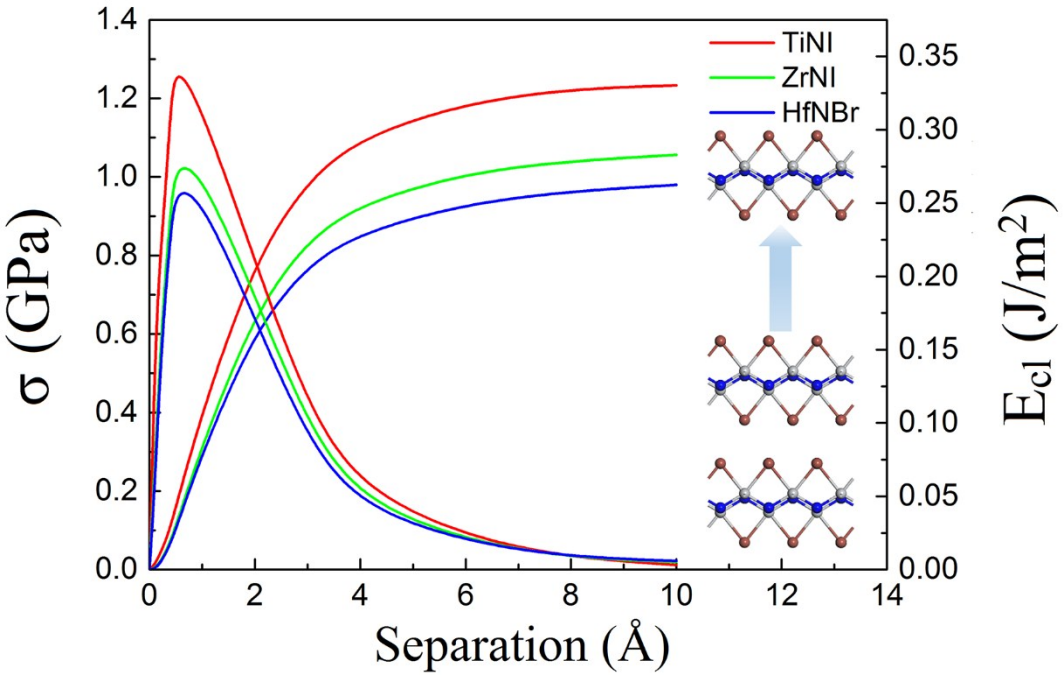

Fig. S11 Cleavage energy E_{cl} (right longitudinal coordinates) and its derivative σ (left longitudinal coordinates) as a function of the separation distance in β-TiNI, β-ZrNI and β-HfNBr bulk. Inset: geometry of introduced fracture.

Table S10. The lattice parameters a, b and c (Å) of β-TiNI, β-ZrNI and β-HfNBr bulk. The numbers in brackets are the experimental data.[2, 3]

	a	b	c
β-TiNI	3.50 (3.51)	3.97 (3.94)	8.88 (8.95)
β-ZrNI	3.74 (3.72)	4.14 (4.11)	9.34 (9.43)
β-HfNBr	3.55 (3.56)	4.11 (4.12)	8.59 (8.64)

References

1. T. J. Booth, P. Blake, R. R. Nair, D. Jiang, E. W. Hill, U. Bangert, A. Bleloch, M. Gass, K. S. Novoselov, M. I. Katsnelson and A. K. Geim, *Nano Lett.*, 2008, **8**, 2442-2446.

2. R. Juza and J. Heners, *Z. Anorg. Allg. Chem.*, 1964, **332**, 159-172.

3. J. Oró-Solé, M. Vlassov, D. Beltrán-Porter, M. T. Caldés, V. Primo and A. Fuertes, *Solid State Sci.*, 2002, **4**, 475-480.